Insights into Self-Poisoning during Catalytic Hydrogenation on Platinum Surfaces using ATR-IR Spectroelectrochemistry

Andrew J. Wain,[1] Michael A. O'Connell [1] and Gary A. Attard [2]*

[1] National Physical Laboratory, Teddington, TW11 0LW, United Kingdom

[2] Department of Physics, The Oliver Lodge Laboratory, University of Liverpool, Liverpool L69 7ZE, United Kingdom

* andy.wain@npl.co.uk , Tel: +44 (0) 20 8943 6243

Abstract

Attenuated total reflection infrared (ATR-IR) spectroscopy has been combined with electrochemical methods to investigate molecular decomposition and self-poisoning processes on platinum surfaces under the conditions of catalytic hydrogenation. In aqueous 0.1 M H_2SO_4 the α-keto ester ethyl pyruvate (EP) is found to decompose on polycrystalline platinum electrodes to yield surface-adsorbed CO but the observed behavior is highly dependent on the electrode potential, a parameter intimately linked to the surface-adsorbed hydrogen coverage. In the potential range −0.2 V to −0.4 V (*vs* mercury/mercurous sulfate electrode) where the hydrogen coverage is negligible, CO is readily produced at the platinum surface along with other molecular fragments but the decomposition process becomes inhibited at high EP solution concentrations. At −0.5 V only very low coverages of CO are observed due to competing hydrogen adsorption at Pt(100) step sites which most favor EP decomposition. At more negative potentials, during the onset of catalytic EP hydrogenation, CO is generated rapidly but other intermediates or products are not observed in the ATR-IR spectra. Together these observations suggest two different mechanisms of EP decomposition, the first occurring directly upon EP adsorption and the second occurring after a single hydrogen atom transfer under hydrogen rich conditions. This ability to control substrate decomposition by tuning the surface hydrogen coverage may be used as a potential route to mitigating catalyst poisoning and deactivation during hydrogenation reactions.

Keywords

Ethyl pyruvate

Dissociation

FTIR spectroscopy

Polycrystalline platinum

Attenuated total reflection

1. Introduction

Catalytic hydrogenations are among the most important transformations in modern chemicals production, accounting for up to 20% of all reaction steps.[1] In particular, these processes feature heavily in the manufacture of pharmaceuticals and specialty chemicals, including flavors, fragrances, vitamins and agrochemicals. Supported metal nanoparticles such as platinum group metals find widespread use as heterogeneous catalysts for such reactions, not only because of their high activity, but their potential for high chemoselectivity.[2-7]

An important step in optimizing selectivity in hydrogenation catalysis is understanding potential side reactions due to both their impact on yield, as well as the potential for catalyst poisoning by undesirable by-products (self-poisoning). A notorious example of this is carbon monoxide (CO), which may be generated *in situ* by dissociation/decarbonylation of substrate molecules, notably alcohols and aldehydes, adsorbed on the catalyst surface.[8-16] Blocking of surface sites by adsorbed CO is recognized as a key mechanism of catalyst deactivation in a wide range of chemical and electrochemical processes, particularly in the case of Pt, which is highly susceptible to CO poisoning by virtue of its strong binding affinity.[17] Such a poison is particularly problematic in catalytic hydrogenation reactions, in which the reducing environment prevents its oxidative removal.[18] Whilst there are many strategies to mitigate CO poisoning, for example by designing bifunctional catalysts with improved CO tolerance,[19,20] minimizing the generation of CO during heterogeneous catalysis is highly desirable. However, the precise mechanism by which CO is formed at the catalyst surface under reaction conditions is often not well understood.

One family of catalytic hydrogenations in which selectivity is of critical importance is asymmetric hydrogenation of prochiral carbonyl compounds. In particular, the enantioselective hydrogenation of α-ketoesters on chirally modified Pt catalysts is of significant interest (see, for example, Scheme 1).[21-30]

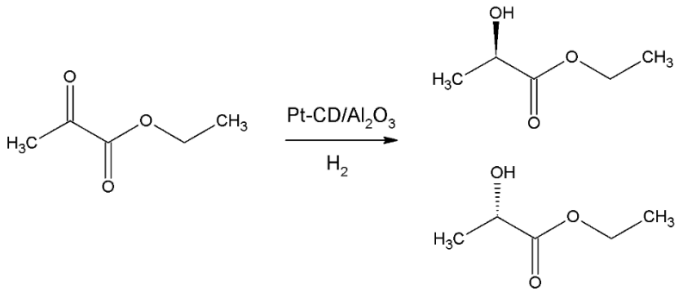

Scheme 1. Enantioselective hydrogenation of ethyl pyruvate to ethyl lactate

Whilst this reaction is known for its high selectivity, adsorbed CO is commonly reported as a decomposition by-product.[31-36] For example, Baiker and co-workers studied the decomposition of the model reactant ethyl pyruvate (EP) on Pt surfaces and concluded that the dissociation reaction likely

occurs across an ensemble of Pt surface atoms.[31] Attard *et al.* later reported that EP decomposition on Pt is a surface sensitive reaction, that is most favored on Pt{100} terraces.[32] Importantly, both authors observed that the adsorption of the chiral modifier cinchonidine (CD) on the Pt surface suppressed the generation of CO. Li *et al*. proposed that adsorbed hydrogen also plays an important role in blocking such side reactions, particularly those associated with the catalyst support.[33] Despite an extensive body of literature on this topic, a complete picture of the route to α-ketoester decomposition and the resulting self-poisoning of Pt during hydrogenation reactions is still lacking.

Electrochemical methods present an attractive approach to probing catalytic reactions at metallic surfaces in aqueous media, and indeed the interaction of EP with Pt surfaces under potential control has received considerable attention.[23,24,32,35-38] Controlling the electrode potential of the catalyst surface not only enables fingerprinting of the vacant surface sites by cyclic voltammetry, but the *in situ* generation of hydrogen at Pt surfaces in aqueous media has been shown to be an attractive approach to simulating hydrogenation conditions for heterogeneous catalysis. Attard and co-workers have used this approach to probe the structure sensitivity of EP adsorption at Pt single crystal electrodes,[32] and later combined electrochemistry with *in situ* Raman spectroscopy to gain molecular insights into the EP hydrogenation reaction.[35-37]

In the present work we extend the above strategy to attenuated total reflection infrared (ATR-IR) spectroscopy, combining it with electrochemistry to explore the adsorptive and self-poisoning behavior of EP on Pt surfaces under hydrogenation conditions. ATR-IR spectroscopy has found considerable use in decomposition studies due to its high sensitivity to carbonyl compounds and in particular surface-adsorbed CO.[39-49] However, the majority of spectroelectrochemical ATR-IR studies in this area have focused on electro-oxidation of small organic molecules, whilst none have examined CO generation in hydrogenative environments. Here we demonstrate that the interaction between EP and polycrystalline Pt exhibits a unique potential dependence which points towards two different mechanisms of decomposition.

2. Experimental Section

2.1 Reagents and Solutions

Electrolyte solutions were prepared by dissolving concentrated sulfuric acid (Sigma-Aldrich, puriss, 95%) in ultrapure water with a resistivity of 18.2 MΩ cm taken from an Elga Purelab Ultra system. Ethyl pyruvate (EP, Sigma-Aldrich, 98%), ethyl-L-lactate (EL, Sigma-Aldrich, 99%), cinchonidine (CD, Sigma-Aldrich, 96%), nitric acid (Sigma-Aldrich, 65%) and hydrochloric acid (Fisher, 37%) were used as received. Electrolyte solutions were degassed with Argon (BOC, 99.998%) before measurements.

2.2 ATR-IR Spectroelectrochemistry

ATR-IR measurements were performed using a Thermo Nicolet iS50 equipped with a liquid nitrogen cooled mercury cadmium telluride (MCT) detector and a Veemax III ATR accessory (Pike Technologies) set to an incidence angle of 60 degrees. Incident light was polarized at 90 degrees using a built-in polarizer. Spectra were recorded with a resolution of 4 cm^{-1} and were typically averaged over 128 acquisitions. Background spectra were either recorded at 0.1 V (*vs* mercury/mercurous sulfate) in the presence of the active organic reagent or in the pure supporting electrolyte at a range of potentials specified in the text. When recording reference spectra, the system was left to equilibrate at the reference potential for at least two minutes.

ATR-IR spectroelectrochemistry was achieved using a modified Pike Technologies electrochemical ATR cell, a schematic depiction of which is shown in Figure 1. Pt thin-film working electrodes were deposited onto a 20 mm diameter silicon internal reflection element (IRE, beveled at 60º, PIKE Technologies) according to the following procedure: (i) the IRE was first cleaned by immersion in aqua regia (3 HCl : 1 HNO_3) followed by sequential ultrasonication in water, isopropyl alcohol and acetone; (ii) the IRE was inserted into a custom-built holder before placing into a Quorum Q150 T turbo-pumped sputter coater; (iii) a 2 nm layer of Cr was deposited onto the IRE in order to improve adhesion; (iv) a 10 nm layer of Pt was then deposited at a rate of 13 nm/min (deposition current 1.25 mA cm^{-2}).

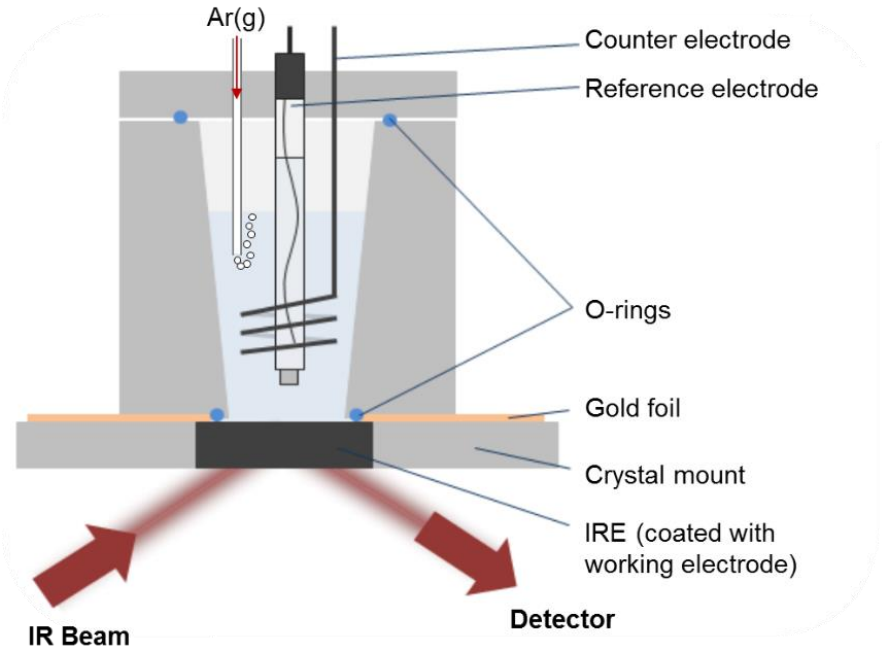

Figure 1. Schematic depiction of electrochemical ATR-IR cell.

Deposited films were characterized by atomic force microscopy (AFM) using an AIST-NT CombiScope-1000SPM AFM system running AIST-NT SPM Control Software (version 3.5.89.2) in tapping mode with Budget Sensors Multi75-AlG probes, which revealed a surface roughness on the order of 1 nm. AFM images of a typical Pt film are shown in Figure S1, in the Supporting Information. Before use, a digital voltmeter was used to check the electrical continuity of the deposited film.

After working electrode deposition and characterization, the Pt-coated IRE was transferred to the ATR crystal mount and electrical connection was made to the top surface by contacting a gold foil around the outer perimeter of the IRE. The electrochemical cell was mounted onto the Pt-coated IRE, using a 15.5 mm inner diameter O-ring to make a liquid-tight seal. A mercury/mercurous sulfate electrode (MSE, sat. K_2SO_4, BAS Inc.) was inserted into the cell as a reference electrode and a Pt wire coil was used as a counter electrode. All potentials are reported against the MSE reference electrode unless otherwise stated, which has a potential of 0.685 V *vs* reversible hydrogen electrode (RHE) in the 0.1 M H_2SO_4 electrolyte solution used in this work. A Perspex lid was fitted to the top of the cell in order to secure the reference and counter electrode in place and allow deaeration of the electrolyte by passing Ar gas (99.998%, BOC Gases) into the cell through a PTFE tube. Electrochemical measurements were performed using a CHI 760C potentiostat (CH Instruments). All experiments were undertaken at 20 ± 2 ºC.

Before any electrochemical or ATR-IR measurements were undertaken it was necessary to increase the active surface area of the Pt film working electrode. This was achieved by potential cycling in 0.1 M H_2SO_4 at 500 mV s^{-1} between –0.7 V and 0.8 V for 5000 cycles. This electrochemical treatment carries the benefit of introducing additional surface defects, which have been shown to play an important role in EP electrochemistry.[32,37] AFM images of a typical Pt film after electrochemical cycling are shown in Figure S1, which exhibit an increase in surface granularity compared to the as-deposited films. Prior to the addition of any organic reagents to the electrochemical cell, the potential was cycled in 0.1 M H_2SO_4 between –0.7 V and 0.5 V in order to electrochemically clean the Pt surface by removing organic contaminants. Cyclic voltammograms (CVs) were typically started at 0 V and scanned initially in the negative direction. During potentiostatic ATR-IR spectroelectrochemical measurements, the potential was not typically taken more negative than –0.7 V, since extended application of more negative potentials led to Pt film damage and delamination.

3. Results and Discussion

3.1 Electrochemistry of Pt films in the absence and presence of EP

Electrochemical characterization of the Pt working electrode was carried out by cyclic voltammetry in 0.1 M H_2SO_4, which exhibited the characteristic features of polycrystalline Pt surface electrochemistry (see Figure 2, black line); hydrogen adsorption/desorption features are observed in the range –0.7 V and –0.4 V whilst oxide formation/reduction takes place between –0.1 V and 0.7 V. Based on the charge associated with hydrogen desorption across four Pt films, the electrochemical surface area of the Pt was estimated to be 3.3 ± 0.3 cm^2, indicating a roughness factor of approximately 1.7. The absence of any abnormal features in the voltammetry suggest that any influence of exposed Cr from the adhesion layer was negligible.

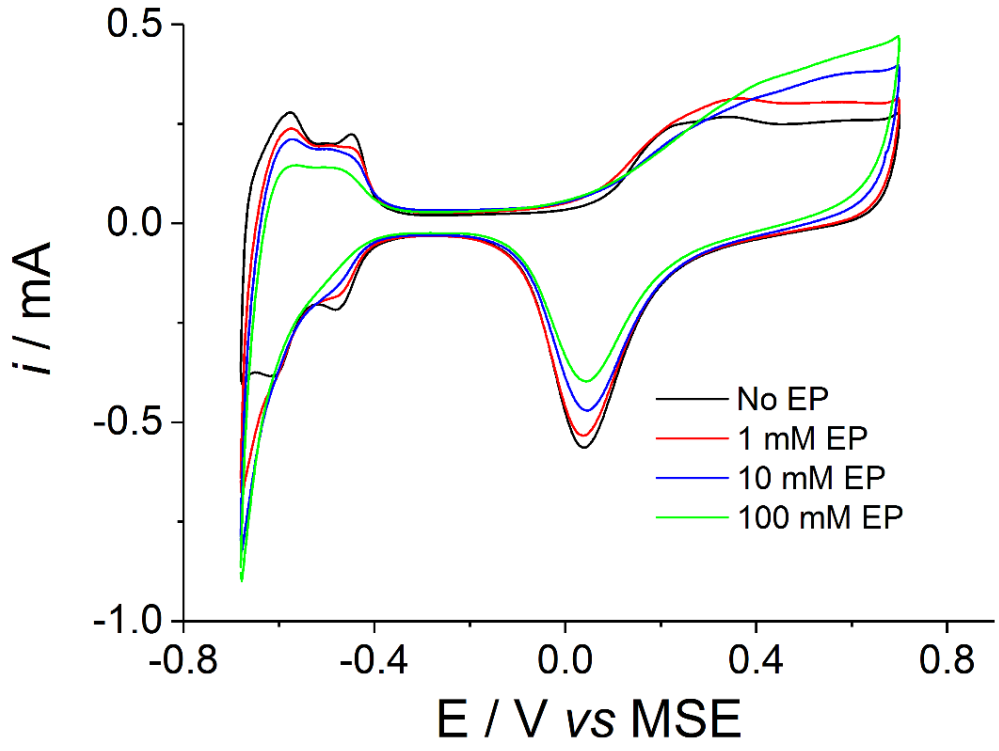

Figure 2. Cyclic voltammetry at 50 mV s^{-1} of Pt film working electrode in 0.1 M H_2SO_4 in the absence of EP and the presence of 1 mM, 10 mM and 100 mM EP (data presented is the third CV scan in each case).

The addition of EP to the electrolyte solution has a notable effect on the voltammetry, as shown in Figure 2. The presence of increasing concentrations of EP results in: (i) gradual attenuation of hydrogen adsorption/desorption peak currents; (ii) significantly increased cathodic currents in the range –0.6 V to –0.7 V; and (iii) additional anodic currents in the range 0.3 V to 0.7 V in the positive scanning direction with a concomitant decrease in the oxide stripping peak current on the return scan. The first of these observations can be attributed to the blocking of the hydrogen adsorption sites by EP. It is noteworthy that the desorption peaks at –0.6 V and –0.45 V, which are associated with Pt{110} and Pt{100} steps respectively, are attenuated most heavily by the presence of EP, whilst the broad underlying Pt{111} desorption feature between –0.7 V and –0.4 V remains present even at 100 mM EP. This is consistent with previous work on Pt single crystals, which indicated that the

relative site blocking affinity of EP on Pt decreases in the order {100}>{110}>>>{111}.[32,37] The emergence of additional reduction currents at the negative limit of the CV has also been observed previously and is associated with the electrochemically-induced catalytic hydrogenation of EP.[35,36] In order to verify this, gas chromatography (GC) analysis was performed on samples of solution after extended periods of electrolysis at −0.7 V, which confirmed generation of the hydrogenation product ethyl lactate (EL) (see Table S1). In the anodic region, the higher currents in the positive scan are most likely related to the electro-oxidation of EP or its electroreduction products, which presumably coincides with the Pt oxide formation, whilst the attenuated currents on the return scan indicate that this process is irreversible. In the following we focus on processes taking place below 0.1 V, since the oxidation of EP is beyond the scope of this work.

3.2 Potentiodynamic ATR-IR Spectroelectrochemistry

In order to better understand the adsorption and catalytic behavior of EP on Pt surfaces under electrochemical conditions, *in situ* ATR-IR spectroscopy was performed. Initial experiments were carried out during a slow CV scan in the presence of 10 mM EP/0.1 M H_2SO_4. The potential was cycled from 0.1 V to −0.7 V and back to 0.1 V at 0.2 mV s^{-1}, and ATR-IR spectra were recorded at 50 mV intervals (background spectrum recorded at 0.1 V). ATR-IR spectra are presented as a 3D waterfall plot in Figure 3a, which reveals a number of interesting features. The positive and negative bands emerging at 3500 cm^{-1} and 3700 cm^{-1} are associated with the restructuring of the metal-aqueous interface upon sweeping the potential and have been discussed in detail elsewhere.[50] The most striking change in the spectrum is the growth of strong positive bands at approximately 2045 cm^{-1} and 1815 cm^{-1}, which are readily assigned respectively to the linear and bridged bonding modes of CO adsorbed on Pt (CO_L and CO_B, respectively).[31] These bands emerge at potentials as positive as −0.1 V and grow considerably as the potential is swept more negative. A slight decrease in CO_L intensity is observed close to −0.7 V before further growth as the scan direction is reversed and finally rapid loss of the CO bands at approximately −0.1 V.

Further spectral features are evident at lower wavenumbers, and their development can be seen more clearly in Figure 3b, which presents the data as a 2D contour plot over a narrower spectral range than Figure 3a. A notable positive band at approximately 1640 cm^{-1} emerges at −0.3 V on the forward CV scan, which is tentatively assigned to a surface carbonyl bond and will be discussed in more detail below. A number of negative spectral features were also observed, including bands at 1176 cm^{-1} and 1113 cm^{-1}, which are associated with the displacement of (bi)sulfate from the metal-electrolyte interface.[51] The origin of the negative bands at 1407 cm^{-1} and 1245 cm^{-1} is unclear at this stage, but may relate to the displacement of alkyl fragments from the surface (*vide infra*).

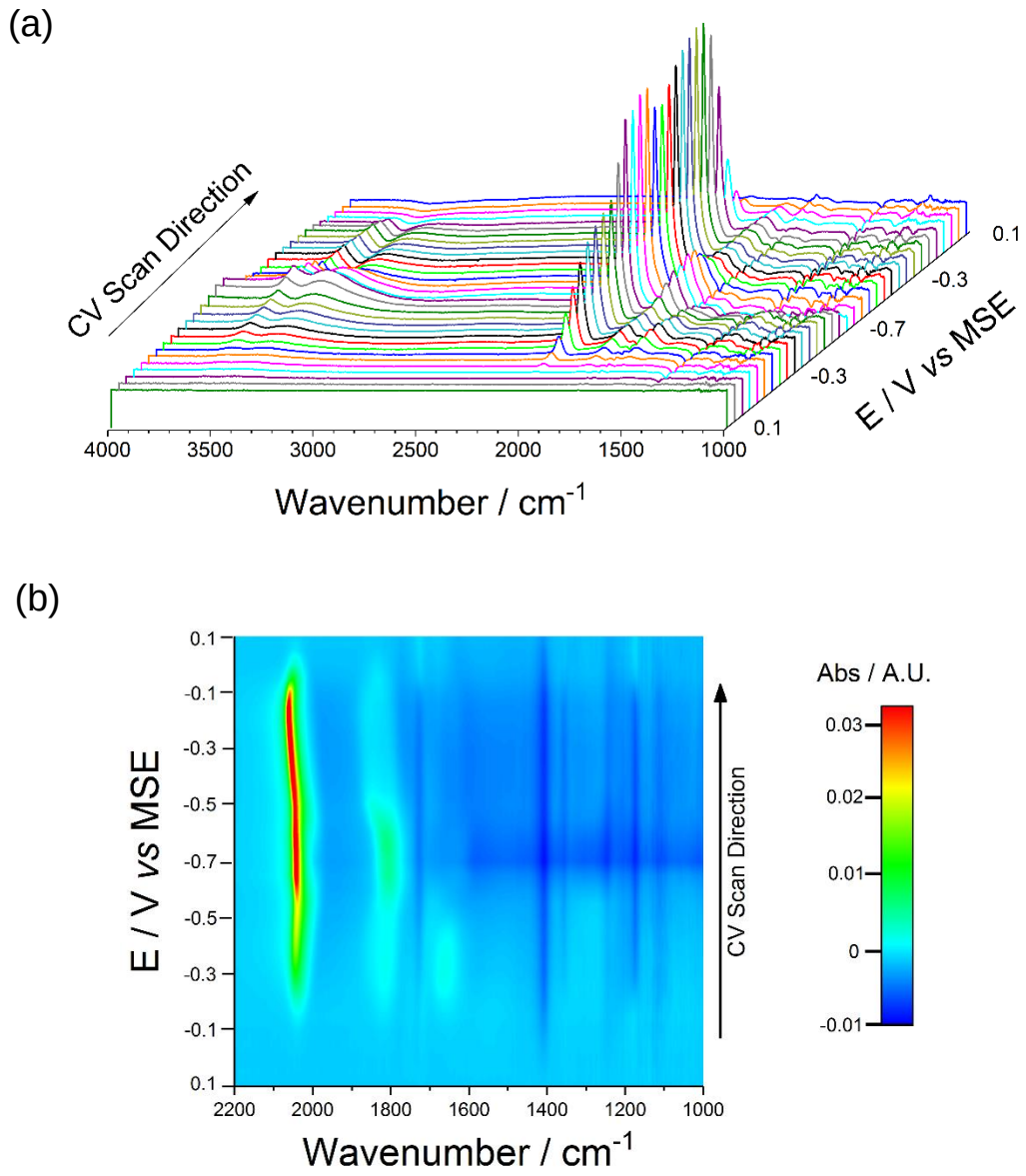

Figure 3. ATR-IR spectra recorded at Pt-film working electrode during a CV scan in the presence of 10 mM EP/0.1 M H_2SO_4 (scan rate 0.2 mV s^{-1}). (a) Full spectral range presented as a 3D waterfall plot. (b) Spectral data presented as a 2D contour plot over a narrower spectral range. Spectra plotted in arbitrary units of absorbance.

It is clear from the above that the ATR-IR spectrum is dominated by the adsorption of CO onto the Pt surface over a wide range of potentials. Control experiments performed in the absence of EP indicated that no CO bands emerged, confirming that EP is the source of the CO. The observation of surface CO by ATR-IR spectroscopy was also reported by Baiker and co-workers who exposed vapor deposited alumina-supported Pt films to EP in H_2-saturated dichloromethane.[31] The origin of the CO is considered to be the dissociation of EP adsorbed at the Pt surface, although the precise fragmentation mechanism is not clear at this stage.

3.2 Potentiostatic ATR-IR Spectroelectrochemistry

In order to investigate the potential and time dependence of this process in more detail, *in situ* ATR-IR measurements were carried out under potentiostatic control. These experiments were performed by beginning with a clean Pt surface immersed in 0.1 M H_2SO_4, adding EP in the concentration range 0.1 – 100 mM, recording an initial reference spectrum at 0.1 V, and then stepping the Pt-film potential to fixed values in the range −0.1 V to −0.65 V. The magnitude of the CO_L and CO_B bands at each of these potentials was observed to increase with time but tended towards a maximum after electrolysis for several tens of minutes. The CO peak intensities and wavenumbers recorded after an equilibration time of 40 mins are plotted in Figure 4 as a function of applied potential for 10 mM EP.

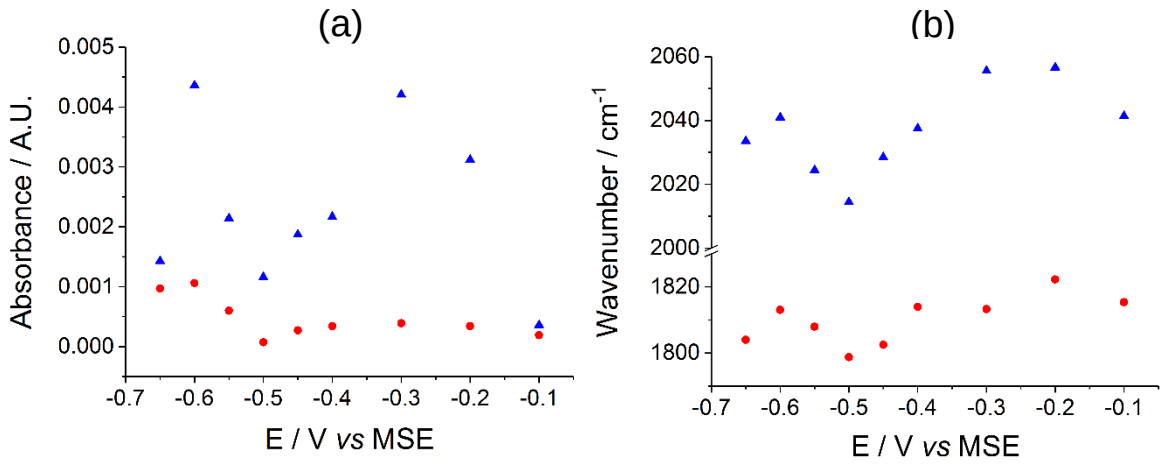

Figure 4. CO peak intensities (a) and wavenumbers (b) recorded as a function of potential during ATR-IR spectroelectrochemistry (10 mM EP/0.1 M H_2SO_4). Blue triangles = CO_L; Red circles = CO_B.

The intensity data in Figure 4a reveal an unusual potential dependence in which the surface CO concentration reaches maxima at approximately −0.3 V and −0.6 V but the band exhibits significant attenuation at −0.5 V. This behavior is most clear from the CO_L band, but is also evident in the CO_B data. However, the low CO_B intensities observed precluded detailed analysis of the CO_L:CO_B ratio. The same trend is also observed in the wavenumber data (Figure 4b), reflecting the shift in CO vibrational frequency with surface concentration. The behavior suggests a competitive adsorption process occurring at −0.5 V which impedes the dissociation of EP to CO. Importantly, equivalent measurements performed with EL, the product of hydrogenating the keto group of EP to the corresponding alcohol, revealed a similar maximum in CO surface concentration at approximately −0.3 V, but no such maximum at −0.6 V (see Figure S2). This implies that the intensity maximum observed at −0.6 V for EP originates from its keto group, whilst that at −0.3 V is associated with the ester group and is therefore common to both EP and EL.

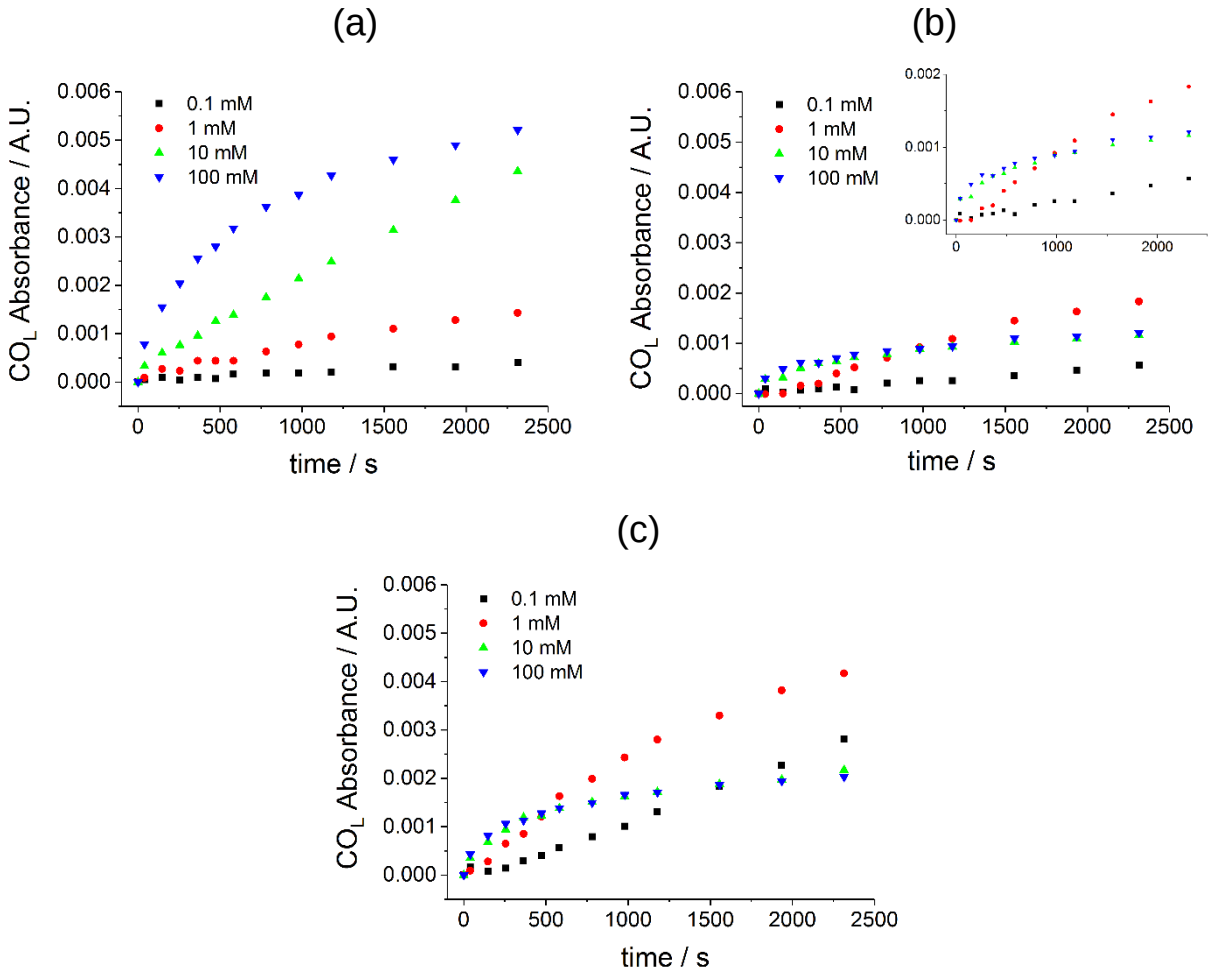

Figure 5. Time series CO_L intensity data for various EP concentrations at (a) –0.6 V, (b) –0.5 V and (c) –0.4 V. Intensity data are plotted on the same scale for comparison. Inset in part (b) shows the same data on a magnified intensity scale.

This unique behavior was probed further through time-series measurements of the CO_L band intensity for a range of EP concentrations (see Figure 5). At –0.6 V (Figure 5a), a simple trend of increasing CO coverage with EP concentration is observed at all times. The curvature of the 100 mM EP data is indicative of the dissociation process tending towards a maximum CO surface coverage. Equivalent measurements in which CO was adsorbed from solution in the absence of EP were consistent with this assertion (Figure S3). The data at –0.5 V (Figure 5b) further highlight the low CO coverage at this potential, but also reveal an interesting variation: whilst the higher two EP concentrations, 10 mM and 100 mM, exhibit higher initial rates of CO generation, over the timescale of this experiment the coverage becomes limited and the curves plateau sooner than the lower concentration (1 mM and 0.1 mM) data. Hence, at long times, the 1 mM EP data actually exhibit higher CO coverages. The

same behavior is observed at −0.4 V (Figure 5c), only with higher absolute CO intensities. In other words, at −0.4 V and −0.5 V the CO generation process appears to be impeded by a high EP solution concentration, which may be linked to competitive EP adsorption on the Pt surface. The fact that the data at −0.6 V show no evidence of this competition is again consistent with an alternative mechanism for dissociation at this potential. Analysis of the initial relative rates, presented in Table S2 and Figure S4, also supports this interpretation. It is important to note that the absolute magnitude of the IR absorbance was found to vary significantly, up to an order of magnitude, across different Pt film working electrodes, reflecting varying levels of surface enhancement associated with differences in Pt surface morphology. However, the data presented in Figures 4 and 5 were collected at the same Pt film, so comparison of the relative CO_L absorbance is reasonable.

Further measurements were performed in the presence of the chiral surface modifier, CD, in order to explore its impact on the EP decomposition process. Figure S5 shows the CO_L signal intensity behavior at CD-modified Pt which exhibits significant attenuation (approximately a factor of 5) compared to clean Pt. This suggests that adsorbed CD impedes EP dissociation, consistent with previous reports that CD suppresses CO formation by blocking the necessary decomposition sites in the Pt surface.[31,52]

3.3 EP Injection Analysis

The potentiostatic ATR-IR experiments discussed above were conducted with the EP present in the solution during the reference spectrum collection at 0.1 V, making detailed spectral analysis of weak bands challenging. In order to assess the development of the more subtle spectral features, experiments were performed in which the reference spectrum was collected at a fixed potential in 0.1 M H_2SO_4 solution the absence of EP, and then a known volume of EP was injected into the cell and ATR-IR spectra recorded at the same potential. The equilibrated spectra are shown in Figure 6, which reveal significant bands at 1714 cm^{-1} and 1661 cm^{-1} for −0.2 V, −0.3 V and −0.4 V. The band at 1714 cm^{-1} is characteristic of a ketone C=O stretch, and is consistent with EP adsorbed to Pt *via* its keto group in an end-on η^1(O) configuration. This band is slightly shifted from the carbonyl band observed in bulk EP at 1725 cm^{-1} (see Figure S6). The more intense band at 1661 cm^{-1} cannot be assigned unambiguously but is most likely associated with the C=O stretch of a η^1(C) carbonyl fragment, such as acetyl and alkoxycarbonyl groups derived *via* scission of the central C-C bond, as reported by Baiker *et al*.[31] Such fragments were observed previously using reflection-absorption infrared spectroscopy (RAIRS) by McBreen *et al.* during methyl pyruvate dissociation Ni(111) surfaces.[53,54] The same authors reported that these surface groups undergo decomposition at above 300 K to generate adsorbed CO, consistent with our observations. The possibility that the 1661 cm^{-1} band is associated with the δ(HOH) bending mode of water co-adsorbed with CO can be ruled out by the absence of a clear ν(OH) stretching band in the region of 3660 cm^{-1} (see Figure S7).[43,50] There is

also a possibility that the 1661 cm^{-1} band is affiliated with the hydrogen-bonded carbonyl group of the enol tautomer of EP. However, the complete absence of a corresponding O–H stretch at between 3600 cm^{-1} and 3400 cm^{-1}, and a C=C stretch at approximately 1630 cm^{-1} suggests this is unlikely. At –0.5 V the carbonyl bands at 1714 cm^{-1} and 1661 cm^{-1} become attenuated whilst at –0.6 V and –0.65 V they vanish entirely, suggesting significant changes in surface coverage or orientation of molecular adsorbates as the potential is shifted to more negative values.

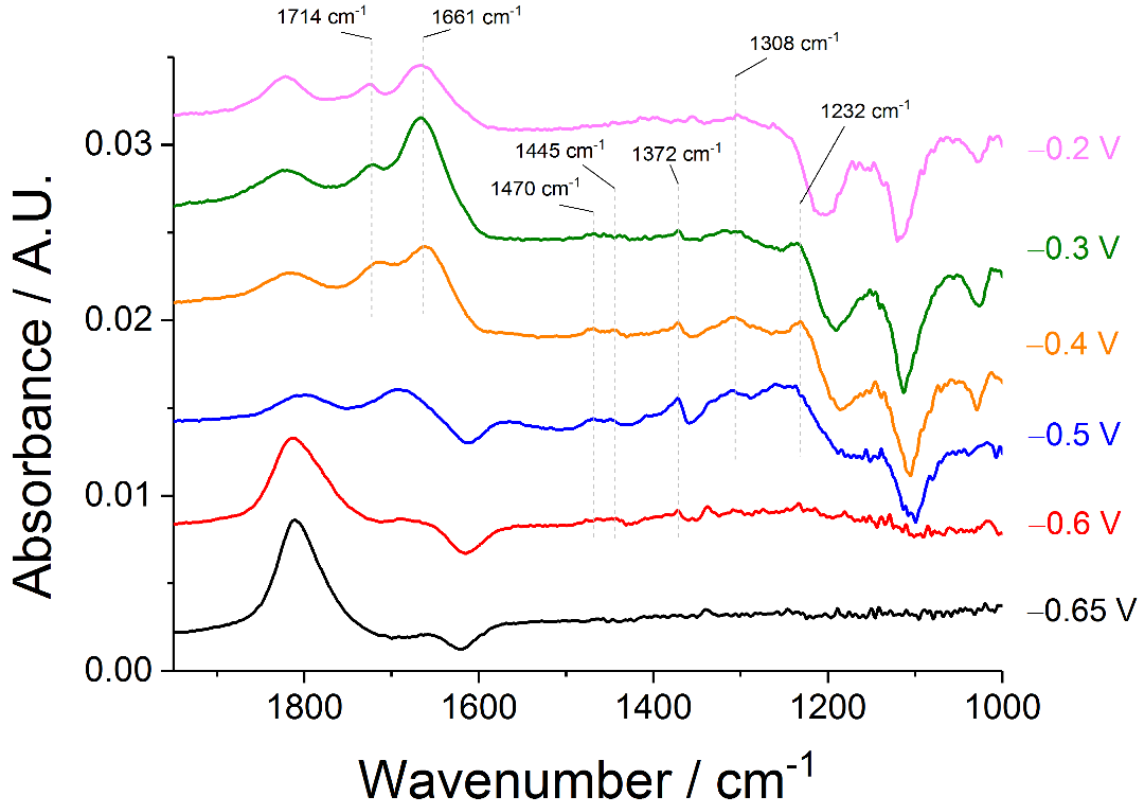

Figure 6. ATR-IR spectra of 10 mM EP injected into 0.1 M H_2SO_4, recorded as a function of potential after an equilibration time of 40 min. Background spectrum recorded before EP injection.

In addition to the relatively strong carbonyl features discussed above, weak but reproducible bands are observed in the fingerprint region at 1470 cm^{-1}, 1445 cm^{-1}, 1372 cm^{-1} and 1308 cm^{-1}, all of which are tentatively ascribed to alkyl CH_2/CH_3 bending vibrations. Based on the ATR spectrum of pure EP,[37] a possible origin of these bands is the ethyl group of the EP ester moiety, the variation in intensity with potential being associated with changes in the molecular orientation (*vide infra*). The slightly higher intensity of the CH_3 bending mode band 1372 cm^{-1} might also suggest an additional contribution from the methyl group of the ketone functionality. It is also possible that these alkyl bands indicate the presence of surface hydrocarbons which accumulate as a by-product of the decomposition process. Bands at 1445 cm^{-1} and 1318 cm^{-1} were also reported during methyl pyruvate dissociation on Ni, and

were ascribed to C2 hydrocarbons formed by C-C coupling of mobile surface CH_3 species, which cannot be ruled out here.[54] Like the carbonyl bands, these alkyl features are found to disappear at –0.6 V and –0.65 V, consistent with these intermediates or side products becoming unstable in the presence of surface adsorbed hydrogen. We note that, with the exception of the primary carbonyl band at

3.4. Adsorption and Dissociation Mechanism

The ATR-IR data presented indicate that the adsorption and dissociation of EP on polycrystalline Pt is highly potential dependent. The CO intensity and time-resolved data suggest that there are two different routes to decomposition, and based on this we propose the mechanism depicted in Scheme 2, discussed below.

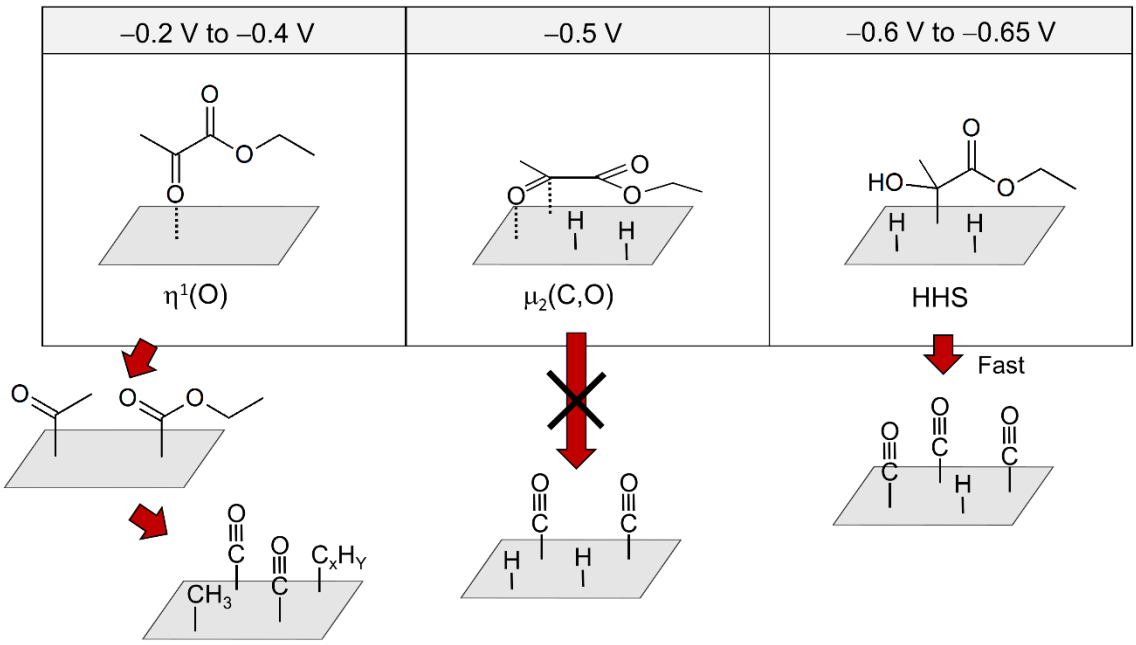

Scheme 2. Schematic depiction of the potential dependence of EP decomposition

The ATR spectra in the potential range –0.2 V to –0.4 V are consistent with EP adsorbed in a η^1(O) configuration co-existing with surface bound acetyl and ethoxycarbonyl groups, hydrocarbon groups and CO. Whilst the carbonyl and hydrocarbon fragments may be spectator species, their observation as reaction intermediates in EP decomposition is highly plausible,[55] although it is not clear exactly how these fragments are initially formed.[54] The steady state coverage of CO in this potential range appears to become limited at high EP concentrations, suggesting a competitive adsorption process, *i.e.* a high EP coverage leads to few available surface sites necessary for the dissociation process. This is consistent with previous work by Baiker *et al.* highlighting the necessity for an ensemble of Pt surface

sites to facilitate decomposition.[31] The surface CO coverage reaches a maximum at −0.3 V, the tail-off at more positive potentials likely being a result of competing (bi)sulfate adsorption, the onset of which is known to occur in this potential range.[56] At approximately 0 V the oxidation of CO on Pt becomes efficient, which is also expected to play a role in the drop in surface CO coverage at more positive potentials.

At potentials more negative than −0.3 V the surface concentration of CO drops and approaches a minimum at approximately −0.5 V. The ATR bands associated with the intermediate EP fragments are also very weak at this potential, suggesting that the above decomposition mechanism becomes impeded. Comparison of the CO intensity data and the CV shown in Figure 2 reveals that the decrease in CO coverage from −0.3 V to −0.5 V coincides with the onset of hydrogen adsorption at the Pt surface. Whilst the hydrogen coverage at this potential is expected to be sub-monolayer, the hydrogen adsorption peak at −0.5 V in the CV is associated with the Pt(100) step edge sites, which have been shown previously to be the most active towards EP decomposition.[32] Hence, the CO intensity minimum at −0.5 V is consistent with adsorbed hydrogen atoms blocking the specific surface sites necessary for EP dissociation. It is also noteworthy that the carbonyl stretch at 1714 cm^{-1} assigned to the η^1(O) adsorbed EP is no longer observed at this potential. We propose that this reflects a change in molecular orientation such that the carbonyl stretch no longer satisfies the required surface selection rules. This observation is in agreement with earlier work using shell isolated nanoparticle enhanced Raman spectroscopy (SHINERS) combined with DFT modelling, which suggested that EP tilts from a η^1(O) bonding mode to a flattened μ_2(C,O) configuration as the potential is taken more negative and the surface becomes populated with hydrogen atoms.[37] Whilst this brings the EP carbon chain into closer proximity to the Pt surface, the co-adsorption of hydrogen still appears to impede its dissociation.

At −0.6 V the CO band intensity increases again and time-resolved measurements indicate that decomposition of EP is facile. The absence of any intermediate carbonyl or hydrocarbon bands in the ATR spectra suggest they are too short lived to be observed, indicating that the dissociation of EP under these conditions is much faster than in the −0.1 V to −0.5 V potential range. Previous work has shown that under hydrogen rich conditions on Pt surfaces, H-atom transfer to EP yields a semi-hydrogenated surface intermediate referred to as the half-hydrogenated state (HHS).[35-37] Since formation of the HHS requires electron transfer between EP and the surface, we postulate that this intermediate is particularly susceptible to dissociation, ultimately into CO. In other words, whilst the co-adsorption of hydrogen blocks dissociation of the μ_2(C,O) EP state at −0.5 V, at more negative potentials the formation of a Pt-C bond promotes rapid decomposition. The HHS was previously identified by a characteristic Raman band at 1050 cm^{-1}. Whilst no such band was observed in the recorded ATR spectra in the present work, this is not unexpected given the poor sensitivity of the

ATR-IR method in this spectral range, as well as the different selection rules for IR compared to Raman spectroscopy. Furthermore, in the work cited above more negative overpotentials were necessary to observe the HHS spectroscopically, but such potentials could not be accessed in the present work due to instabilities in the Pt film electrode.

The formation of the HHS is followed by a second H-atom transfer to generate the fully hydrogenated product, EL, which can easily desorb from the Pt surface. This turnover of EP and H-atoms at the Pt surface results in the dynamic release of surface sites, thus facilitating a high rate of decomposition of adjacent HHS intermediates and a rapid accumulation of surface CO. At even more negative potentials (–0.65 V, close to the onset of hydrogen evolution), the rate of H-atom transfer to EP is expected to increase, leading to a high steady-state concentration of the HHS, as observed previously.[35-37] It is likely that at sufficiently negative potentials this accumulation of the HHS and the ensuing hydrogenation begins to impede the dissociation process due to the blocking of surface sites, thus leading to a decrease in the steady state surface CO concentration at –0.65 V. This hypothesis is supported by chemical analysis of EP solutions after sustained electrolysis at hydrogen evolution potentials, which showed unequivocal catalytic turnover to produce the hydrogenation product, EL (see Supporting Information section S2).

Importantly, equivalent spectroelectrochemical experiments performed with EL, rather than EP, fully support the above interpretation. EL is susceptible to decomposition between –0.2 V and –0.4 V, presumably *via* a similar mechanism to EP, which must therefore involve the ester functionality. EL also exhibits the same decrease in CO intensity at –0.5 V due to competitive hydrogen adsorption. However, EL does not exhibit an increase in CO intensity at –0.6 V to –0.65 V because it is already hydrogenated and therefore does not generate a HHS, thus precluding decomposition at these potentials.

4. Conclusions

By combining electrochemical methods with *in situ* ATR-IR we have shown that the dissociation of molecular adsorbates on Pt electrodes to produce surface-bound CO can occur *via* multiple distinct pathways, and that the dominant route depends highly on electrode potential. In the case of EP in aqueous acid solutions, there are two different mechanisms of decomposition. At potentials in the range –0.2 V to –0.4 V acetyl, ethoxycarbonyl and hydrocarbon groups accumulate on the surface, presumably *via* initial scission of the central C–C bond after EP physisorption. High solution phase concentrations of EP limit this process due to the resulting high surface EP coverage and low availability of vacant Pt surface sites necessary for dissociation. Similarly, hydrogen adsorption at more negative potentials significantly blocks the dissociation process. However, when the surface

hydrogen coverage is sufficient for EP to undergo semi-hydrogenation to the HHS, the Pt–C bond formation provides an alternative low-barrier pathway to dissociation and the dynamic turnover of surface EP and H atoms facilitates rapid decomposition.

Whilst the aqueous and potential-controlled conditions of the spectroelectrochemical measurements performed in this work differ from those typically encountered in heterogeneous catalysis, these observations have important implications for catalytic hydrogenation reactions. The −0.2 V to −0.4 V regime can be compared to a Pt catalyst exposed to EP in the absence of hydrogen, under which conditions surface CO generation is expected. However, the co-adsorption of hydrogen clearly has a significant influence on this process and the present work has shown that very small changes in surface hydrogen coverage can lead to quite dramatic changes in decomposition behavior. The implication is that the "low hydrogen coverage" dissociation pathway can be minimized, understandably, by ensuring high substrate concentrations and not allowing hydrogen-lean conditions to arise. The data also strongly suggest that the decomposition side reaction could be significantly inhibited by site-selective surface blocking strategies, however such an approach would likely have a negative impact on overall hydrogenation rate, as well as enantioselectivity.

Finally, the present work has highlighted the value of combined spectroelectrochemical ATR-IR measurements in revealing molecular insights into heterogeneous catalysis at solid-liquid interfaces, and in particular gleaning a better understanding of catalyst deactivation as a consequence of decomposition or decarbonylation side reactions.

Author Information

Corresponding Author:

* AJW: email, andy.wain@npl.co.uk, tel, +44 (0) 20 8943 6243

Notes:

The authors declare no competing financial interest.

Associated Content

Supporting Information:

AFM Imaging of Pt Films

Gas Chromatography Analysis of Catalytic Conversion

Potential Dependence of CO Generation from Ethyl Lactate

CO Adsorption from Solution

Initial Rates of EP Decomposition

Time Series ATR-IR Measurements in the Presence of Cinchonidine (CD)

Bulk FTIR Spectra of EP and EL

EP Injection Analysis at High Wavenumbers

Acknowledgements

The authors thank the UK National Measurement System (Department of Business, Energy & Industrial Strategy) for financial support.

References

(1) Nerozzi, F., Heterogeneous Catalytic Hydrogenation. *Platinum Met. Rev.* **2012**, *56*, 236-241.

(2) Zhu, Y. J.; Zaera, F., Selectivity in the Catalytic Hydrogenation of Cinnamaldehyde Promoted by Pt/Sio2 as a Function of Metal Nanoparticle Size. *Catal. Sci. Technol.* **2014**, *4*, 3390-3390.

(3) Vargas, A.; Reimann, S.; Diezi, S.; Mallat, T.; Baiker, A., Adsorption Modes of Aromatic Ketones on Platinum and Their Reactivity Towards Hydrogenation. *J. Mol. Catal. A: Chem.* **2008**, *282*, 1-8.

(4) Bidaoui, M.; Especel, C.; Bouchenafa-Saib, N.; Duprez, D.; Mohammedi, O.; Royer, S., Citral Hydrogenation on High Surface Area Mesoporous Tio2-Sio2 Supported Pt Nanocomposites: Effect of Titanium Loading and Reduction Temperature on the Catalytic Performances. *Applied Catalysis a-General* **2012**, *445*, 14-25.

(5) Bucsi, I.; Sutyinszki, M.; Felfoldi, K.; Bartok, M., Hydrogenation of Beta-Isocinchonicine in Mild Conditions on Pt and Pd Catalysts Using Hplc-Esi-Ion-Trap Ms: New Results on the Role of Structure of Cinchona Alkaloids in the Orito Reaction. *Catal. Commun.* **2006**, *7*, 104-108.

(6) Tang, Y.; Miao, S. J.; Pham, H. N.; Datye, A.; Zheng, X. M.; Shanks, B. H., Enhancement of Pt Catalytic Activity in the Hydrogenation of Aldehydes. *Applied Catalysis a-General* **2011**, *406*, 81-88.

(7) Taylor, M. J.; Jiang, L.; Reichert, J.; Papageorgiou, A. C.; Beaumont, S. K.; Wilson, K.; Lee, A. F.; Barth, J. V.; Kyriakou, G., Catalytic Hydrogenation and Hydrodeoxygenation of Furfural over Pt(111): A Model System for the Rational Design and Operation of Practical Biomass Conversion Catalysts. *J. Phys. Chem. C* **2017**, *121*, 8490-8497.

(8) Davis, J. L.; Barteau, M. A., Decarbonylation and Decomposition Pathways of Alcohols on Pd(111). *Surf. Sci.* **1987**, *187*, 387-406.

(9) Shekhar, R.; Barteau, M. A.; Plank, R. V.; Vohs, J. M., Adsorption and Reaction of Aldehydes on Pd Surfaces. *The Journal of Physical Chemistry B* **1997**, *101*, 7939-7951.

(10) Brown, N. F.; Barteau, M. A., Reactions of Unsaturated Oxygenates on Rhodium(111) as Probes of Multiple Coordination of Adsorbates. *J. Am. Chem. Soc.* **1992**, *114*, 4258-4265.

(11) Singh, U. K.; Vannice, M. A., Liquid-Phase Citral Hydrogenation over SiO2-Supported Group Viii Metals. *J. Catal.* **2001**, *199*, 73-84.

(12) Grass, M. E.; Rioux, R. M.; Somorjai, G. A., Dependence of Gas-Phase Crotonaldehyde Hydrogenation Selectivity and Activity on the Size of Pt Nanoparticles (1.7–7.1 nm) Supported on Sba-15. *Catal. Lett.* **2009**, *128*, 1-8.

(13) Pushkarev, V. V.; Musselwhite, N.; An, K.; Alayoglu, S.; Somorjai, G. A., High Structure Sensitivity of Vapor-Phase Furfural Decarbonylation/Hydrogenation Reaction Network as a Function of Size and Shape of Pt Nanoparticles. *Nano Lett.* **2012**, *12*, 5196-5201.

(14) Zhang, X.; Durndell, L. J.; Isaacs, M. A.; Parlett, C. M. A.; Lee, A. F.; Wilson, K., Platinum-Catalyzed Aqueous-Phase Hydrogenation of D-Glucose to D-Sorbitol. *ACS Catalysis* **2016**, *6*, 7409-7417.

(15) Taylor, M. J.; Durndell, L. J.; Isaacs, M. A.; Parlett, C. M. A.; Wilson, K.; Lee, A. F.; Kyriakou, G., Highly Selective Hydrogenation of Furfural over Supported Pt Nanoparticles under Mild Conditions. *Applied Catalysis B: Environmental* **2016**, *180*, 580-585.

(16) de Jesús, J. C.; Zaera, F., Adsorption and Thermal Chemistry of Acrolein and Crotonaldehyde on Pt(111) Surfaces. *Surf. Sci.* **1999**, *430*, 99-115.

(17) Ertl, G.; Neumann, M.; Streit, K. M., Chemisorption of Co on the Pt(111) Surface. *Surf. Sci.* **1977**, *64*, 393-410.

(18) Rylander, P. *Catalytic Hydrogenation over Platinum Metals*; Academic Press: London, 1967, p 20-21.

(19) Lee, M. J.; Kang, J. S.; Kang, Y. S.; Chung, D. Y.; Shin, H.; Ahn, C.-Y.; Park, S.; Kim, M.-J.; Kim, S.; Lee, K.-S.; Sung, Y.-E., Understanding the Bifunctional Effect for Removal of Co Poisoning: Blend of a Platinum Nanocatalyst and Hydrous Ruthenium Oxide as a Model System. *ACS Catalysis* **2016**, *6*, 2398-2407.

(20) Liu, H.; Li, Y.; Luque, R.; Jiang, H., A Tuneable Bifunctional Water-Compatible Heterogeneous Catalyst for the Selective Aqueous Hydrogenation of Phenols. *Adv. Synth. Catal.* **2011**, *353*, 3107-3113.

(21) Baiker, A., Progress in Asymmetric Heterogeneous Catalysis: Design of Novel Chirally Modified Platinum Metal Catalysts. *J. Mol. Catal. A: Chem.* **1997**, *115*, 473-493.

(22) Baiker, A., Catalysis on Chiral Surfaces. *Catal. Sci. Technol.* **2015**, *5*, 636-637.

(23) Jenkins, D. J.; Alabdulrahman, A. M. S.; Attard, G. A.; Griffin, K. G.; Johnston, P.; Wells, P. B., Enantioselectivity and Catalyst Morphology: Step and Terrace Site Contributions to Rate and Enantiomeric Excess in Pt-Catalysed Ethyl Pyruvate Hydrogenation. *J. Catal.* **2005**, *234*, 230-239.

(24) Attard, G. A.; Griffin, K. G.; Jenkins, D. J.; Johnston, P.; Wells, P. B., Enantioselective Hydrogenation of Ethyl Pyruvate Catalysed by Pt/Graphite: Superior Performance of Sintered Metal Particles. *Catal. Today* **2006**, *114*, 346-352.

(25) Blaser, H. U.; Jalett, H. P.; Spindler, F., Enantioselective Hydrogenation of Alpha-Ketoesters: Comparison of Homogeneous and Heterogeneous Catalysts. *J. Mol. Catal. A: Chem.* **1996**, *107*, 85-94.

(26) Blaser, H. U.; Jalett, H. P.; Muller, M.; Studer, M., Enantioselective Hydrogenation of Alpha-Ketoesters Using Cinchona Modified Platinum Catalysts and Related Systems: A Review. *Catal. Today* **1997**, *37*, 441-463.

(27) Bonello, J. M.; Lambert, R. M.; Kunzle, N.; Baiker, A., Platinum-Catalyzed Enantioselective Hydrogenation of Alpha-Ketoesters: An Unprecedented Surface Reaction of Methyl Pyruvate. *J. Am. Chem. Soc.* **2000**, *122*, 9864-9865.

(28) Szollosi, G.; Cserenyi, S.; Balazsik, K.; Fulop, F.; Bartok, M., New Data in the Enantioselective Hydrogenation of Ethyl Pyruvate on Pt-Cinchona Chiral Catalyst Using Continuous-Flow Fixed-Bed Reactor System: The Origin of Rate Enhancement. *J. Mol. Catal. A: Chem.* **2009**, *305*, 155-160.

(29) Schmidt, E.; Vargas, A.; Mallat, T.; Baiker, A., Shape-Selective Enantioselective Hydrogenation on Pt Nanoparticles. *J. Am. Chem. Soc.* **2009**, *131*, 12358-12367.

(30) Blaser, H. U.; Jalett, H. P.; Wiehl, J., Enantioselective Hydrogenation of A-Ketoesters with Cinchona-Modified Platinum Catalysts: Effect of Acidic and Basic Solvents and Additives. *J. Mol. Catal.* **1991**, *68*, 215-222.

(31) Ferri, D.; Burgi, T.; Baiker, A., The Fate of Ethyl Pyruvate During Adsorption on Platinum Chirally Modified by Cinchonidine Studied by Atr-Ir Spectroscopy. *J. Phys. Chem. B* **2004**, *108*, 14384-14391.

(32) Hazzazi, O. A.; Huxter, S. E.; Taylor, R.; Palmer, B.; Gilbert, L.; Attard, G. A., Electrochemical Studies of Irreversibly Adsorbed Ethyl Pyruvate on Pt{H K L} and Epitaxial Pd/Pt{H K L} Adlayers. *J. Electroanal. Chem.* **2010**, *640*, 8-16.

(33) Liu, Z.; Li, X.; Ying, P.; Feng, Z.; Li, C., Fourier Transform Infrared Spectroscopic Study on the Adsorption of Ethyl Pyruvate on Pt/Al2o3: Side Reactions Suppressed by Adsorbed Hydrogen and Cinchonidine. *J. Phys. Chem. C* **2007**, *111*, 823-829.

(34) Ferri, D.; Diezi, S.; Maciejewski, M.; Baiker, A., Alumina-Catalysed Degradation of Ethyl Pyruvate During Enantioselective Hydrogenation over Pt/Alumina and Its Inhibition by Acetic Acid. *Appl. Catal., A* **2006**, *297*, 165-173.

(35) Rees, N. V.; Taylor, R. J.; Jiang, Y. X.; Morgan, I. R.; Knight, D. W.; Attard, G. A., In Situ Surface-Enhanced Raman Spectroscopic Studies and Electrochemical Reduction of Alpha-Ketoesters and Self Condensation Products at Platinum Surfaces. *J. Phys. Chem. C* **2011**, *115*, 1163-1170.

(36) Taylor, R. J.; Jiang, Y. X.; Rees, N. V.; Attard, G. A.; Jeffery, E. L.; Willock, D. J., Enantioselective Hydrogenation of Alpha-Ketoesters: An in Situ Surface-Enhanced Raman Spectroscopy (Sers) Study. *J. Phys. Chem. C* **2011**, *115*, 21363-21372.

(37) Guan, S. L.; Donovan-Sheppard, O.; Reece, C.; Willock, D. J.; Wain, A. J.; Attard, G. A., Structure Sensitivity in Catalytic Hydrogenation at Platinum Surfaces Measured by Shell-Isolated Nanoparticle Enhanced Raman Spectroscopy (Shiners). *ACS Catalysis* **2016**, *6*, 1822-1832.

(38) Attard, G. A.; Gillies, J. E.; Harris, C. A.; Jenkins, D. J.; Johnston, P.; Price, M. A.; Watson, D. J.; Wells, P. B., Electrochemical Evaluation of the Morphology and Enantioselectivity of Pt/Graphite. *Appl. Catal., A* **2001**, *222*, 393-405.

(39) Zhang, Y.; Tong, Y.; Lu, L.; Osawa, M.; Ye, S., Dme Dissociation Reaction on Platinum Electrode Surface: A Quantitative Kinetic Analysis by in Situ Ir Spectroscopy. *J. Electrochem. Soc.* **2010**, *157*, F10-F15.

(40) Wang, Q.; Sun, G. Q.; Jiang, L. H.; Xin, Q.; Sun, S. G.; Jiang, Y. X.; Chen, S. P.; Jusys, Z.; Behm, R. J., Adsorption and Oxidation of Ethanol on Colloid-Based Pt/C, Ptru/C and Pt3sn/C Catalysts: In Situ Ftir Spectroscopy and on-Line Dems Studies. *PCCP* **2007**, *9*, 2686-2696.

(41) Heinen, M.; Jusys, Z.; Behm, R. J., Ethanol, Acetaldehyde and Acetic Acid Adsorption/Electrooxidation on a Pt Thin Film Electrode under Continuous Electrolyte Flow: An in Situ Atr-Ftirs Flow Cell Study. *The Journal of Physical Chemistry C* **2010**, *114*, 9850-9864.

(42) Schnaidt, J.; Heinen, M.; Denot, D.; Jusys, Z.; Behm, R. J., Electrooxidation of Glycerol Studied by Combined in Situ Ir Spectroscopy and Online Mass Spectrometry under Continuous Flow Conditions. *J. Electroanal. Chem.* **2011**, *661*, 250-264.

(43) Schnaidt, J.; Heinen, M.; Jusys, Z.; Behm, R. J., Electro-Oxidation of Ethylene Glycol on a Pt-Film Electrode Studied by Combined in Situ Infrared Spectroscopy and Online Mass Spectrometry. *J. Phys. Chem. C* **2012**, *116*, 2872-2883.

(44) Schnaidt, J.; Jusys, Z.; Behm, R. J., Electrooxidation of 1-Propanol on Pt - Mechanistic Insights from a Spectro-Electrochemical Study Using Isotope Labeling. *J. Phys. Chem. C* **2012**, *116*, 25852-25867.

(45) Schnaidt, J.; Heinen, M.; Jusys, Z.; Behm, R. J., Oxidation of the Partly Oxidized Ethylene Glycol Oxidation Products Glycolaldehyde, Glyoxal, Glycolic Acid, Glyoxylic Acid, and Oxalic Acid on Pt Electrodes: A Combined Atr-Ftirs and Dems Spectroelectrochemical Study. *J. Phys. Chem. C* **2013**, *117*, 12689-12701.

(46) Reichert, R.; Schnaidt, J.; Jusys, Z.; Behm, R. J., The Influence of Reactive Side Products on the Electrooxidation of Methanol - a Combined in Situ Infrared Spectroscopy and Online Mass Spectrometry Study. *PCCP* **2014**, *16*, 13780-13799.

(47) Keresszegi, C.; Ferri, D.; Mallat, T.; Baiker, A., On the Role of Co Formation During the Aerobic Oxidation of Alcohols on Pd/Al2o3: An in Situ Attenuated Total Reflection Infrared Study. *J. Catal.* **2005**, *234*, 64-75.

(48) Busó-Rogero, C.; Brimaud, S.; Solla-Gullon, J.; Vidal-Iglesias, F. J.; Herrero, E.; Behm, R. J.; Feliu, J. M., Ethanol Oxidation on Shape-Controlled Platinum Nanoparticles at Different Phs: A Combined in Situ Ir Spectroscopy and Online Mass Spectrometry Study. *J. Electroanal. Chem.* **2016**, *763*, 116-124.

(49) Burgener, M.; Wirz, R.; Mallat, T.; Baiker, A., Nature of Catalyst Deactivation During Citral Hydrogenation: A Catalytic and Atr-Ir Study. *J. Catal.* **2004**, *228*, 152-161.

(50) Osawa, M.; Tsushima, M.; Mogami, H.; Samjeske, G.; Yamakata, A., Structure of Water at the Electrified Platinum-Water Interface: A Study by Surface-Enhanced Infrared Absorption Spectroscopy. *J. Phys. Chem. C* **2008**, *112*, 4248-4256.

(51) Iwasita, T.; Nart, F. C., In Situ Infrared Spectroscopy at Electrochemical Interfaces. *Prog. Surf. Sci.* **1997**, *55*, 271-340.

(52) Hazzazi, O. A.; Harris, C. A.; Wells, P. B.; Attard, G. A., Electrooxidation of D- and L-Glucose at Well-Defined Chiral Bimetallic Electrodes. *Top. Catal.* **2011**, *54*, 1392-1402.

(53) Castonguay, M.; Roy, J. R.; Lavoie, S.; Adnot, A.; McBreen, P. H., Selective C-C Bond Activation of Methyl Pyruvate on Ni(111) to Yield Surface Methoxycarbonyl. *J. Am. Chem. Soc.* **2001**, *123*, 6429-6430.

(54) Castonguay, M.; Roy, J. R.; Lavoie, S.; Laliberte, M. A.; McBreen, P. H., Methyl Pyruvate on Ni(111): Coverage-Dependent Thermal Chemistry. *J. Phys. Chem. B* **2004**, *108*, 4134-4140.

(55) Davis, J. L.; Barteau, M. A., Spectroscopic Identification of Alkoxide, Aldehyde, and Acyl Intermediates in Alcohol Decomposition on Pd(111). *Surf. Sci.* **1990**, *235*, 235-248.

(56) Kolics, A.; Wieckowski, A., Adsorption of Bisulfate and Sulfate Anions on a Pt(111) Electrode. *The Journal of Physical Chemistry B* **2001**, *105*, 2588-2595.

Table of Contents Graphic